Published in International Journal of Solids and Structures 96 (2016)1-10.

Effective behavior of a microscopically damaged interface between a layer and a half-space occupied by dissimilar piezoelectric media under antiplane deformations

W. T. Ang*, X. Wang and H. Fan
School of Mechanical and Aerospace Engineering,
Nanyang Technological University, Singapore

Abstract

The present paper examines the effective macroscopic behavior of a microscopically damaged interface between an infinitely long piezoelectric layer and a piezoelectric half-space under antiplane deformation. The interface is modeled as containing a periodic array of micro-cracks. The lengths and the positions of the micro-cracks on a period interval of the interface are randomly generated. The micro-statistical model is formulated in terms of hypersingular integral equations and used to investigate in detail the influences of the material constants of the piezoelectric layer and the half-space and the width of the layer on the effective properties of the interface.

Keywords: Weak interface, micro-statistical model, effective properties, piezoelectric materials, hypersingular integral equations.

*Author for correspondence, mwtang@ntu.edu.sg

1 Introduction

The macro-level generalized spring-like model for a weak interface Γ between two piezoelectric materials denoted by 1 and 2 is given by the interfacial conditions

$$\left.\begin{array}{l} \underline{\underline{\boldsymbol{\sigma}}}^{(1)} \bullet \underline{\mathbf{n}} = \underline{\underline{\boldsymbol{\sigma}}}^{(2)} \bullet \underline{\mathbf{n}} = \underline{\underline{\mathbf{a}}} \bullet (\underline{\mathbf{u}}^{(1)} - \underline{\mathbf{u}}^{(2)}) + \underline{\mathbf{b}}\,(\phi^{(1)} - \phi^{(2)}) \\ \underline{\mathbf{D}}^{(1)} \bullet \underline{\mathbf{n}} = \underline{\mathbf{D}}^{(2)} \bullet \underline{\mathbf{n}} = \underline{\mathbf{c}} \bullet (\underline{\mathbf{u}}^{(1)} - \underline{\mathbf{u}}^{(2)}) + h(\phi^{(1)} - \phi^{(2)}) \end{array}\right\} \text{ on } \Gamma, \qquad (1)$$

where $\underline{\mathbf{n}}$ is the unit normal vector to Γ pointing into material 1, $\underline{\mathbf{u}}^{(i)}$ and $\underline{\underline{\boldsymbol{\sigma}}}^{(i)}$ are respectively the displacement and the stress in material i, $\phi^{(i)}$ and $\underline{\mathbf{D}}^{(i)}$ are respectively the electrical potential and the electrical displacement in material i and the scalar h, the vectors $\underline{\mathbf{b}}$ and $\underline{\mathbf{c}}$ and the second rank tensor $\underline{\underline{\mathbf{a}}}$ are tensorial quantities characterizing the effective properties of Γ.

The spring-like model has been proposed and used by many researchers for analyzing weak interfaces in elastic layered materials (Benveniste and Miloh [3], Hashin [7], Jones and Whittier [8], López-Realpozo et al. [13], Pilarski and Rose [16] and Rokhlin and Wang [17]) as well as in piezoelectric layered materials (Li and Lee [10, 11, 12], Wang and Pan [23], Wang et al. [24] and Wang and Sudak [25]). For the case of piezoelectric layered materials, most (if not all) of the existing papers made the assumption that no coupling exists between the displacement and electrical potential jumps in the interfacial conditions, that is, they assumed that $\underline{\mathbf{b}} = \underline{\mathbf{0}}$ and $\underline{\mathbf{c}} = \underline{\mathbf{0}}$ in (1). The validity of such an assumption may be checked by using micro-models to estimate the effective properties of microscopically damaged interfaces.

As is clear from the reference [8] above, there are, however, few research papers on micro-analyses for estimating the effective properties of micro-damaged interfaces between dissimilar materials. Fan and Sze [4] studied the effective electrical behavior of a micro-cracked interface between dielectric materials by using a finite-element based three-phase model. More recently,

Wang et al. [20, 21, 22] proposed a micro-statistical model for estimating the effective stiffness of a micro-damaged interface between dissimilar materials under elastostatic deformations.

The current paper adopts the micro-statistical approach to analyze the effective properties of a micro-damaged interface between an infinitely long piezoelectric layer and a piezoelectric half-space under antiplane deformation. As in [20, 21, 22], the interface is modeled as containing a periodic array of micro-cracks which are taken to be either electrically impermeable or permeable. The lengths and the positions of the micro-cracks on a period interval of the interface are randomly generated. The boundary conditions on the micro-cracks are expressed in terms of hypersingular integral equations which are solved numerically. Once the hypersingular integral equations are solved, quantities describing the effective properties of the interface can be readily estimated. The influences of the material constants of the piezoelectric layer and the half-space and the width of the layer on the effective properties of the interface are examined in detail.

The problem under consideration here may be of practical interest as piezoelectric thin film structures are widely used in microelectronics (Park el al. [14, 15] and Trolier-McKinstry and Muralt [19]). Such a structure is formed by coating a thin layer of piezoelectric material on a substrate of dissimilar material (see Tateyama el al. [18]). The interface between the thin layer and the substrate may be damaged by a distribution of micro-cracks. For a simpler mathematical analysis of the layered piezoelectric structure, the interface may be modeled using (1). Unless the edge of the layer is very far away from the micro-cracks, its effects on the effective properties of the micro-cracked interface cannot be ignored in the modeling of the interface.

2 The problem and basic equations

With reference to a Cartesian coordinate system $Ox_1x_2x_3$, consider a thin piezoelectric layer occupying the region $0 < x_2 < h$ (h is a positive constant) bonded to a piezoelectric half-space in the region $x_2 < 0$. The layer and the half-space are occupied possibly dissimilar materials. The interface $x_2 = 0$ between the thin layer and the half-space is microscopically damaged. The geometries of the piezoelectric bimaterial are independent of the spatial coordinate x_3.

The micro-damaged interface is modeled as containing a periodic array of micro-cracks. Specifically, a period interval of the interface contains M arbitrarily located micro-cracks of possibly different lengths. In the region $0 < x_1 < L$, $x_2 = 0$, the tips of the m-th micro-cracks are given by $(a^{(m)}, 0)$ and $(b^{(m)}, 0)$, where $a^{(m)}$ and $b^{(m)}$ ($m = 1, 2, \cdots, M$) are real numbers such that $0 < a^{(1)} < b^{(1)} < a^{(2)} < b^{(2)} < \cdots < a^{(M)} < b^{(M)} < L$. The micro-cracks on the remaining part of the interface are given by $a^{(m)}+nL < x_1 < b^{(m)}+nL$ for $m = 1, 2, \cdots, M$ and $n = \pm 1, \pm 2, \cdots$, that is, the remaining parts of the interface are periodically distributed replicas of the region $0 < x_1 < L$, $x_2 = 0$. Refer to Figure 1 for a geometrical sketch of the piezoelectric bimaterial having three micro-cracks ($M = 3$) over a period interval of the interface.

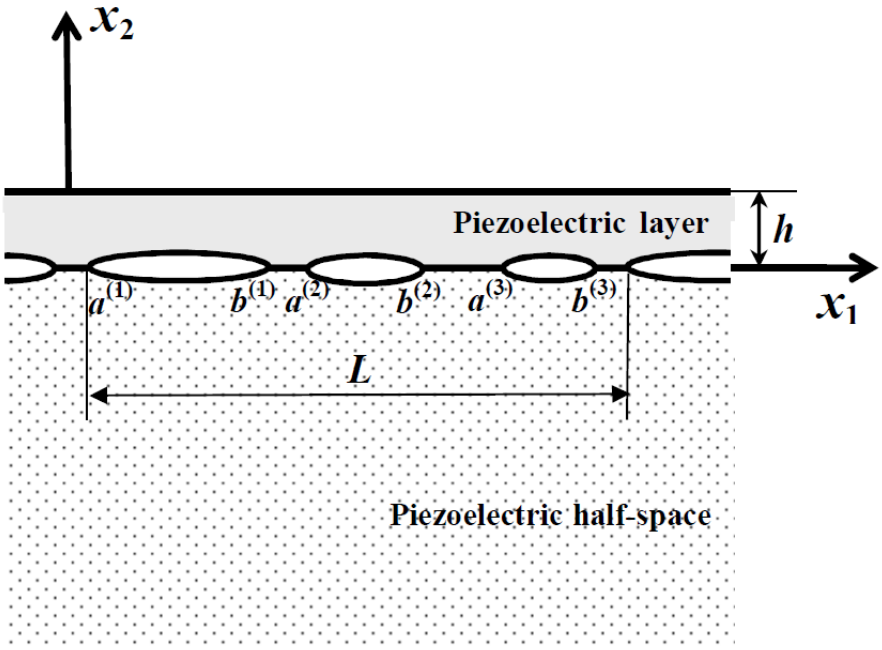

Figure 1. A sketch of the geometry of the piezoelectric bimaterial for $M = 3$.

The damage ratio (or micro-crack density) ρ of the interface is defined by

$$\rho = \frac{1}{L}\sum_{k=1}^{M}(b^{(k)} - a^{(k)}). \tag{2}$$

The piezoelectric bimaterial undergoes an antiplane deformation with electrical poling in the x_3 direction. The only non-zero component of the Cartesian displacement is u_3 which is a function of only x_1 and x_2. The antiplane stresses σ_{3k} and the electric displacements D_k are given by (see, for

example, Auld [2] and Li and Lee [11])

$$\begin{aligned} \sigma_{3k} &= c_{44}(x_2)\frac{\partial u_3}{\partial x_k} + e_{15}(x_2)\frac{\partial \phi}{\partial x_k}, \\ D_k &= e_{15}(x_2)\frac{\partial u_3}{\partial x_k} - \epsilon_{11}(x_2)\frac{\partial \phi}{\partial x_k}, \end{aligned} \tag{3}$$

where ϕ is the electrical potential which is also a function of only x_1 and x_2, and $c_{44}(x_2)$, $e_{15}(x_2)$ and $\epsilon_{11}(x_2)$ are respectively the elastic moduli, piezoelectric coefficient and dielectric coefficient of the piezoelectric bimaterial given by

$$\begin{aligned} &(c_{44}(x_2), e_{15}(x_2), \epsilon_{11}(x_2)) \\ = &\begin{cases} (c_{44}^{(1)}, e_{15}^{(1)}, \epsilon_{11}^{(1)}) & \text{for } 0 < x_2 < h, \\ (c_{44}^{(2)}, e_{15}^{(2)}, \epsilon_{11}^{(2)}) & \text{for } x_2 < 0, \end{cases} \end{aligned} \tag{4}$$

with $c_{44}^{(n)}, e_{15}^{(n)}$ and $\epsilon_{11}^{(n)}$ $(n = 1, 2)$ being suitably given constants.

According to the law of conservation of momentum and the Gauss law of electric flux, the antiplane deformation of the piezoelectric bimaterial is governed by the partial differential equations

$$\begin{aligned} \frac{\partial^2}{\partial x_k \partial x_k}(c_{44}(x_2)u_3 + e_{15}(x_2)\phi) &= 0, \\ \frac{\partial^2}{\partial x_k \partial x_k}(e_{15}(x_2)u_3 - \epsilon_{11}(x_2)\phi) &= 0. \end{aligned} \tag{5}$$

Note that the Einsteinian convention of summing over repeated indices applies for lower case Latin subscripts which run from 1 to 2.

For the antiplane deformation, the generalized spring-like model in (1) for the micro-cracked interface $x_2 = 0$ between the piezoelectric layer and the piezoelectric half-space can be re-written as

$$\begin{bmatrix} \sigma_{32}(x_1, 0^+) \\ D_2(x_1, 0^+) \end{bmatrix} = \begin{bmatrix} \sigma_{32}(x_1, 0^-) \\ D_2(x_1, 0^-) \end{bmatrix} = \begin{bmatrix} k_{11} & k_{12} \\ k_{21} & k_{22} \end{bmatrix} \begin{bmatrix} \Delta u_3(x_1) \\ \Delta \phi(x_1) \end{bmatrix} \quad \text{for } -\infty < x_1 < \infty, \tag{6}$$

where $\Delta u_3(x_1) = u_3(x_1, 0^+) - u_3(x_1, 0^-)$, $\Delta\phi(x_1) = \phi(x_1, 0^+) - \phi(x_1, 0^-)$ and k_{ij} are coefficients characterizing the effective piezoelectric properties of the interface.

The problem of interest here is to estimate the effective properties k_{ij} of the interface by taking into consideration the details of the interfacial micro-cracks.

For the macro-level model in (6), the interfacial micro-cracks are taken to be electrically impermeable. Thus, there is a jump in the electrical potential ϕ across the interface.

However, if the interfacial micro-cracks are electrically permeable, the electrical potential ϕ is continuous on the interface. For an electrically permeable interface, the interfacial conditions in (6) for the generalized spring-like model should be modified to become

$$\left.\begin{array}{rcl} \sigma_{32}(x_1, 0^+) = \sigma_{32}(x_1, 0^-) & = & k\Delta u_3(x_1) \\ D_2(x_1, 0^+) - D_2(x_1, 0^-) & = & 0 \\ \phi(x_1, 0^+) - \phi(x_1, 0^-) & = & 0 \end{array}\right\} \text{for } -\infty < x_1 < \infty, \qquad (7)$$

where k is the effective stiffness of the interface to be estimated.

3 Hypersingular integral formulation

For mathematical convenience, we introduce the generalized displacements U_I and stresses S_{Ik} $(I = 1, 2;\ k = 1, 2)$

$$\begin{array}{rcl} U_1 & = & u_3,\ U_2 = \phi,\ S_{1k} = \sigma_{3k},\ S_{2k} = D_k, \\ C_{1k1p} & = & c_{44}\delta_{kp},\ C_{1k2p} = e_{15}\delta_{kp},\ C_{2k1p} = e_{15}\delta_{kp},\ C_{2k2p} = -\varepsilon_{11}\delta_{kp} \end{array} \qquad (8)$$

and rewrite (3) and (5) as

$$S_{Kj} = C_{KjRp}\frac{\partial U_R}{\partial x_p} \text{ for } K,\ j = 1, 2, \qquad (9)$$

and

$$C_{KiRp}\frac{\partial^2 U_R}{\partial x_j \partial x_p} = 0 \text{ for } K = 1, 2. \tag{10}$$

The convention of summing over repeated indices also applies for upper case Latin subscripts running from 1 to 2.

The boundary value problem for the micro-cracked interface described in Section 2 requires solving (10) in the piezoelectric bimaterial subject to the conditions

$$\left.\begin{array}{rcl} S_{K2}(x_1, h) & = & 0 \\ S_{K2}(x_1, 0^+) & = & S_{K2}(x_1, 0^-) \end{array}\right\} \text{ for } -\infty < x_1 < \infty,$$
$$\Delta U_K(x_1) = 0 \text{ for points } (x_1, 0) \text{ outside micro-cracks,}$$
$$S_{Kj}(x_1, x_2) \to 0 \text{ as } x_2 \to -\infty, \tag{11}$$

and

$$S_{K2}(x_1, 0) = -P_K(x_1)$$
$$\text{for points } (x_1, 0) \text{ on electrically impermeable micro-cracks,} \tag{12}$$

where $\Delta U_K(x_1) = U_K(x_1, 0^+) - U_K(x_1, 0^-)$ and $P_K(x_1)$ are suitably prescribed internal loads acting on the micro-cracks. The internal loads $P_K(x_1)$ are periodic functions of x_1 with period L. For the analysis here, they are taken to be constants. For the far-field conditions in (11), we require the generalized stresses to decay as $O(|x_2|^{-\alpha})$ for large $|x_2|$, where α is a real number such that $\alpha > 1$.

In Wang et al. [21], the same boundary value problem was solved for a micro-cracked interface between an orthotropic elastic layer and an orthotropic half-space under inplane deformations. The hypersingular integral equations for (10) together with (11) and (12) can be extracted from [21].

They are given by

$$\begin{aligned}
&\frac{1}{2\pi}\fint_0^L U_R(x_1,h)G_{RI}[\frac{1}{(x_1-\xi_1)^2}+\Theta(x_1,\xi_1)]dx_1\\
&+\frac{1}{2\pi}\int_0^L U_R(x_1,h)H_{RI}\,\mathrm{Re}\{\Omega(x_1,\xi_1,2ih)\}dx_1\\
&-\frac{1}{2\pi}\sum_{k=1}^{M}\int_{a^{(k)}}^{b^{(k)}}\Delta U_R(x_1)G_{RI}\,\mathrm{Re}\{\Omega(x_1,\xi_1,-ih)\}dx_1\\
&-\frac{1}{2\pi}\sum_{k=1}^{M}\int_{a^{(k)}}^{b^{(k)}}\Delta U_R(x_1)H_{RI}\,\mathrm{Re}\{\Omega(x_1,\xi_1,ih)\}dx_1\\
=\;& 0 \;\text{ for } 0<\xi_1<L, \qquad (13)
\end{aligned}$$

and

$$\begin{aligned}
&-\frac{1}{2\pi}\int_0^L U_R(x_1,h)W_{RI}\,\mathrm{Re}\{\Omega(x_1,\xi_1,ih)\}dx_1\\
&+\frac{1}{2\pi}[\fint_{a^{(k)}}^{b^{(k)}}\frac{\Delta U_R(x_1)W_{RI}}{(x_1-\xi_1)^2}dx_1\\
&+\sum_{\substack{n=1\\n\neq k}}^{M}\int_{a^{(n)}}^{b^{(n)}}\frac{\Delta U_R(x_1)W_{RI}}{(x_1-\xi_1)^2}dx_1\\
&+\sum_{n=1}^{M}\int_{a^{(n)}}^{b^{(n)}}\Delta U_R(x_1)W_{RI}\Theta(x_1,\xi_1)dx_1]\\
=\;& P_I(\xi_1)\text{ for } a^{(k)}<\xi_1<b^{(k)}\ (k=1,2,...,M). \qquad (14)
\end{aligned}$$

where $\fint$ denotes that the integral is to be interpreted in the Hadamard finite-part sense, $i=\sqrt{-1}$, $W_{RI}=G_{RI}+H_{RI}$, G_{RI} and H_{RI} are constants defined by

$$[G_{RI}]=\begin{bmatrix} -c_{44}^{(1)} & -e_{15}^{(1)} \\ -e_{15}^{(1)} & \epsilon_{11}^{(1)} \end{bmatrix}, \qquad (15)$$

$$
\begin{aligned}
H_{11} &= -H_0 c_{44}^{(1)}[(c_{44}^{(2)} - c_{44}^{(1)})(\epsilon_{11}^{(1)} + \epsilon_{11}^{(2)}) - (e_{15}^{(1)} + e_{15}^{(2)})^2] \\
&\quad -2H_0[c_{44}^{(1)}(e_{15}^{(2)})^2 + c_{44}^{(2)}(e_{15}^{(1)})^2], \\
H_{12} &= H_{21} = -H_0 e_{15}^{(1)}(c_{44}^{(1)} - c_{44}^{(2)})(\epsilon_{11}^{(1)} - \epsilon_{11}^{(2)}) \\
&\quad +H_0(e_{15}^{(1)} - e_{15}^{(2)})[2c_{44}^{(1)}\epsilon_{11}^{(1)} + e_{15}^{(1)}(e_{15}^{(1)} + e_{15}^{(2)})], \\
H_{22} &= H_0\epsilon_{11}^{(1)}[(c_{44}^{(2)} + c_{44}^{(1)})(\epsilon_{11}^{(2)} - \epsilon_{11}^{(1)}) - (e_{15}^{(1)} + e_{15}^{(2)})^2] \\
&\quad +2H_0[\epsilon_{11}^{(1)}(e_{15}^{(2)})^2 + \epsilon_{11}^{(2)}(e_{15}^{(1)})^2], \\
H_0 &= \frac{1}{(c_{44}^{(1)} + c_{44}^{(2)})(\epsilon_{11}^{(1)} + \epsilon_{11}^{(2)}) + (e_{15}^{(1)} + e_{15}^{(2)})^2},
\end{aligned} \tag{16}
$$

and $\Theta(x_1, \xi_1)$ and $\Omega(x_1, \xi_1, z)$ are defined by

$$
\begin{aligned}
\Theta(x_1, \xi_1) &= \frac{1}{L^2}\Psi_1(\frac{L + x_1 - \xi_1}{L}) + \frac{1}{L^2}\Psi_1(\frac{L + \xi_1 - x_1}{L}), \\
\Omega(x_1, \xi_1, z) &= \frac{1}{(x_1 - \xi_1 + z)^2} + \frac{1}{L^2}\Psi_1(\frac{L + x_1 - \xi_1 + z}{L}) \\
&\quad +\frac{1}{L^2}\Psi_1(\frac{L - x_1 + \xi_1 - z}{L}),
\end{aligned} \tag{17}
$$

with Ψ_1 being the trigamma function.

To compute the coefficients k_{ij} in (6) for the effective properties of the weak interface modeled using electrically impermeable micro-cracks, the hypersingular integral equations are solved numerically for $\Delta U_R(x_1)$ as described in Wang et al. [21] for two independent set of loads $P_I = P_I^{(1)}$ and $P_I = P_I^{(2)}$. If the solution corresponding to $P_I = P_I^{(q)}$ is given by $\Delta U_R^{(q)}(x_1)$ then k_{ij} can be determined by solving the system

$$
\begin{bmatrix} k_{11} & k_{12} \\ k_{21} & k_{22} \end{bmatrix} \sum_{k=1}^{M} \int_{a^{(k)}}^{b^{(k)}} \begin{bmatrix} \Delta U_1^{(q)}(x_1) \\ \Delta U_2^{(q)}(x_1) \end{bmatrix} dx_1 = \int_0^L \begin{bmatrix} P_1^{(q)}(x_1) \\ P_2^{(q)}(x_1) \end{bmatrix} dx_1 \text{ for } q = 1, 2. \tag{18}
$$

For more details on numerical methods for hypersingular integral equations, refer to Ang [1].

If the micro-cracks are electrically permeable, the boundary conditions in

(12) are replaced by

$$\Delta U_2(x_1) = 0 \text{ for } -\infty < x_1 < \infty,$$
$$S_{12}(x_1, 0) = -P_1(x_1)$$
$$\text{for points } (x_1, 0) \text{ on electrically permeable micro-cracks,} \quad (19)$$

and the corresponding hypersingular integral equations are given by (13) for $I = 1, 2$, and (14) for $I = 1$ (only) together with $\Delta U_2 = 0$. Once the integral equations are solved for $\Delta U_1(x_1)$, the effective stiffness k in (7), for the interface weakened by electrically permeable cracks, can be estimated from

$$k \sum_{k=1}^{M} \int_{a^{(k)}}^{b^{(k)}} \Delta U_1(x_1) dx_1 = \int_0^L P_1(x_1) dx_1. \quad (20)$$

For the special case $h \to \infty$ (that is, the case where the micro-cracked interface lies between two half-spaces), the hypersingular integral equations in (13) and (14) for electrically impermeable micro-cracks reduce to

$$\begin{aligned} & \frac{1}{2\pi} [\neq\!\!\!\int_{a^{(k)}}^{b^{(k)}} \frac{\Delta U_R(x_1) W_{RI}}{(x_1 - \xi_1)^2} dx_1 \\ & + \sum_{\substack{n=1 \\ n \neq k}}^{M} \int_{a^{(n)}}^{b^{(n)}} \frac{\Delta U_R(x_1) W_{RI}}{(x_1 - \xi_1)^2} dx_1 \\ & + \sum_{n=1}^{M} \int_{a^{(n)}}^{b^{(n)}} \Delta U_R(x_1) W_{RI} \Theta(x_1, \xi_1) dx_1] \\ = \; & P_I(\xi_1) \text{ for } a^{(k)} < \xi_1 < b^{(k)} \; (k = 1, 2, ..., M), \end{aligned} \quad (21)$$

and the hypersingular integral equations for electrically permeable micro-

cracks are given by

$$\begin{aligned}
&\frac{1}{2\pi}[\neq\int_{a^{(k)}}^{b^{(k)}} \frac{\Delta U_1(x_1)W_{11}}{(x_1-\xi_1)^2}dx_1 \\
&+\sum_{\substack{n=1\\n\neq k}}^{M}\int_{a^{(n)}}^{b^{(n)}} \frac{\Delta U_1(x_1)W_{11}}{(x_1-\xi_1)^2}dx_1 \\
&+\sum_{n=1}^{M}\int_{a^{(n)}}^{b^{(n)}} \Delta U_1(x_1)W_{11}\Theta(x_1,\xi_1)dx_1] \\
= \;& P_1(\xi_1) \text{ for } a^{(k)}<\xi_1<b^{(k)} \ (k=1,2,...,M). \qquad (22)
\end{aligned}$$

For such a case, by directly comparing (21) and (22) for constant loads P_I, we may easily see that

$$\frac{\Delta U_1^{(\mathrm{imp})}(x_1)}{P_1T_{11}+P_2T_{21}} = \frac{\Delta U_2^{(\mathrm{imp})}(x_1)}{P_1T_{12}+P_2T_{22}} = \frac{\Delta U_1^{(\mathrm{per})}(x_1)W_{11}}{P_1}, \qquad (23)$$

where $[T_{RJ}]$ is the inverse of $[W_{RJ}]$, $\Delta U_I^{(\mathrm{imp})}(x_1)$ and $\Delta U_1^{(\mathrm{per})}(x_1)$ are respectively the generalized displacement jumps for the electrically impermeable and permeable micro-cracks. From (21), (22) and (23), we may deduce that the effective stiffness coefficient k_{11} in (18) (for electrically impermeable interface) is equal to the effective stiffness k in (20) (for electrically permeable interface) for the special case where $h \to \infty$.

4 Statistical approach

The statistical approach in Wang et al. [22], which takes into account the random positions and sizes of the micro-cracks, is adopted here to estimate the effective properties of the micro-cracked interface.

The lengths of the M micro-cracks over the period interval $0 < x_1 < L$, $x_2 = 0$ are randomly generated to follow the χ^2 distribution of a particular degree of freedom p, that is, $\chi^2(p)$. For a more realistic simulation of the

micro-crack length variation, a low degree of freedom, like $p = 5$, is used in the χ^2 distribution, so that a greater number of shorter micro-cracks are generated. Once the lengths are generated, the micro-cracks are randomly positioned over the period interval to form a micro-cracked interface.

To estimate the effective properties of micro-cracked interfaces, N interfaces, each having the same number of micro-cracks and the same damage ratio, are randomly generated to form a statistical sample. The effective properties of each of the N interfaces in the statistical sample are calculated for fixed values of $c_{44}^{(n)}, e_{15}^{(n)}$ and $\epsilon_{11}^{(n)}$ $(n = 1, 2)$ and $h/\widehat{a}$ (h is the width of the piezoelectric layer and $2\widehat{a}$ is the average length of the micro-cracks on the interface) as explained in Section 3.

The non-dimensionalized effective properties $\widehat{a}k_{11}/C_{44}^{(2)}$, $\widehat{a}k_{12}/\sqrt{C_{44}^{(2)}\epsilon_{11}^{(2)}}$, $\widehat{a}k_{21}/\sqrt{C_{44}^{(2)}\epsilon_{11}^{(2)}}$ and $\widehat{a}k_{22}/(-\epsilon_{11}^{(2)})$ have values $K_{11}^{(n)}$, $K_{12}^{(n)}$, $K_{21}^{(n)}$ and $K_{22}^{(n)}$ respectively for the n-th interface in the statistical sample of N interfaces damaged by electrically impermeable micro-cracks. The non-dimensionalized effective properties are estimated using the mean $\widehat{K}_{ij}$ with standard deviation s_{ij}, where

$$\widehat{K}_{ij} = \frac{1}{N}\sum_{n=1}^{N} K_{ij}^{(n)} \text{ and } s_{ij} = \sqrt{\frac{1}{N-1}\sum_{n=1}^{N}(K_{ij}^{(n)} - \widehat{K}_{ij})^2}. \tag{24}$$

Similarly, for the statistical sample of N interfaces damaged by electrically permeable micro-cracks, if non-dimensionalized effective stiffness $\widehat{a}k/C_{44}^{(2)}$ of the n-th interface are given by $K^{(n)}$, then the mean value $\widehat{K}$ and the corresponding standard deviation s of the non-dimensionalized effective stiffness coefficient are respectively given by

$$\widehat{K} = \frac{1}{N}\sum_{n=1}^{N} K^{(n)} \text{ and } s = \sqrt{\frac{1}{N-1}\sum_{n=1}^{N}(K^{(n)} - \widehat{K})^2}. \tag{25}$$

5 Number of micro-cracks required for homogenizing the interface

For a sufficiently large sample of interfaces (like $N = 50$), the average values $\widehat{K}_{ij}$ and $\widehat{K}$ calculated in (24) and (25) are found not to vary significantly with M (the number of micro-cracks on a period interval of an interface) when M exceeds a certain positive integer.

For the purpose of illustration, we take the thin layer to be occupied by the dielectric material Germanium with material constants $C_{44}^{(1)} = 6.71 \times 10^{10}$ N/m^2, $e_{15}^{(1)} = 0.00$ C/m^2 and $\epsilon_{11}^{(1)} = 1.47 \times 10^{-10}$ C/(V m) (Gurzadyan and Tzankov [5]) and the half-space by the piezoelectric material ZnO with the material constants $C_{44}^{(2)} = 4.25 \times 10^{10}$ N/m^2, $e_{15}^{(2)} = 0.48$ C/m^2 and $\epsilon_{11}^{(2)} = 0.76 \times 10^{-10}$ C/(V m) (Li and Gupta [9]).

For $\rho = 0.5$ and $h/\widehat{a} = 1$, we generate a sample of 50 interfaces, each damaged by M micro-cracks per period interval of the interface. The lengths of the micro-cracks vary according to the $\chi^2(5)$ distribution. We investigate how the average means of $\widehat{a}k_{11}/C_{44}^{(2)}$, $\widehat{a}k_{12}/\sqrt{C_{44}^{(2)}\epsilon_{11}^{(2)}}$, $\widehat{a}k_{21}/\sqrt{C_{44}^{(2)}\epsilon_{11}^{(2)}}$ and $\widehat{a}k_{22}/(-\epsilon_{11}^{(2)})$ (for electrically impermeable micro-cracks) and $\widehat{a}k/C_{44}^{(2)}$ (for electrically permeable micro-cracks), as computed by using the interfaces in the sample, vary with M. For a given value of M, scatter plot of the data of the non-dimensionalized effective properties for the 50 interfaces damaged by electrically impermeable micro-cracks and the mean of the data are shown in Figures 2, 3 and 4. (Note that $k_{12} = k_{21}$.) Similar scatter plots and the means of the non-dimensional effective stiffness of the 50 interfaces damaged by electrically permeable interfaces are shown in Figure 5.

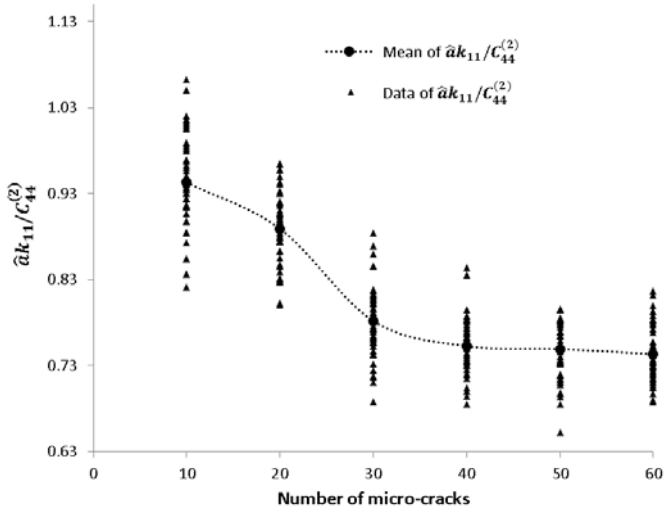

Figure 2. Scatter plots of the data of $\widehat{a}k_{11}/C_{44}^{(2)}$ and plots of the mean of the data for different values of M.

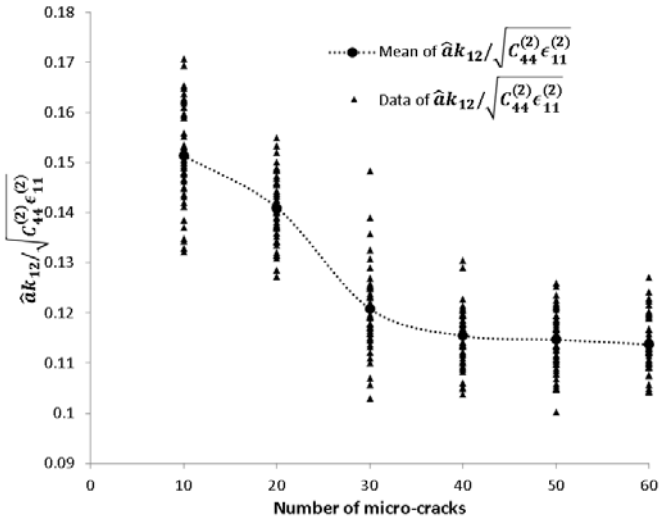

Figure 3. Scatter plots of the data of $\widehat{a}k_{12}/\sqrt{C_{44}^{(2)}\epsilon_{11}^{(2)}}$ and plots of the mean of the data for different values of M.

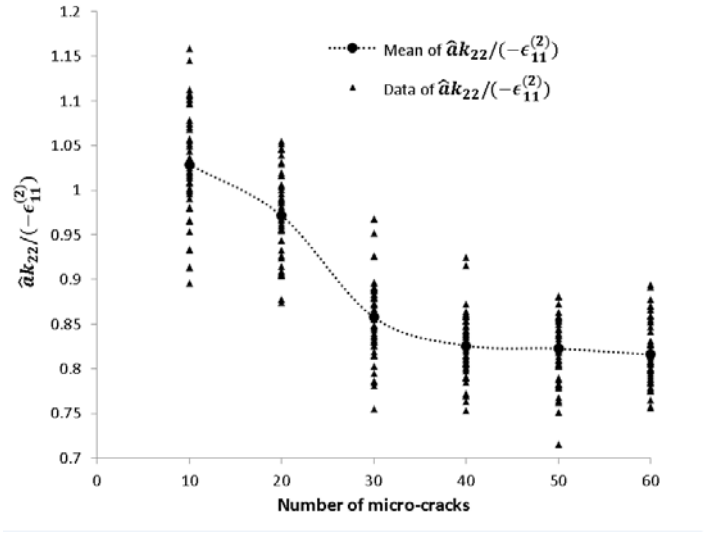

Figure 4. Scatter plots of the data of $\widehat{a}k_{22}/(-\epsilon_{11}^{(2)})$ and plots of the mean of the data for different values of M.

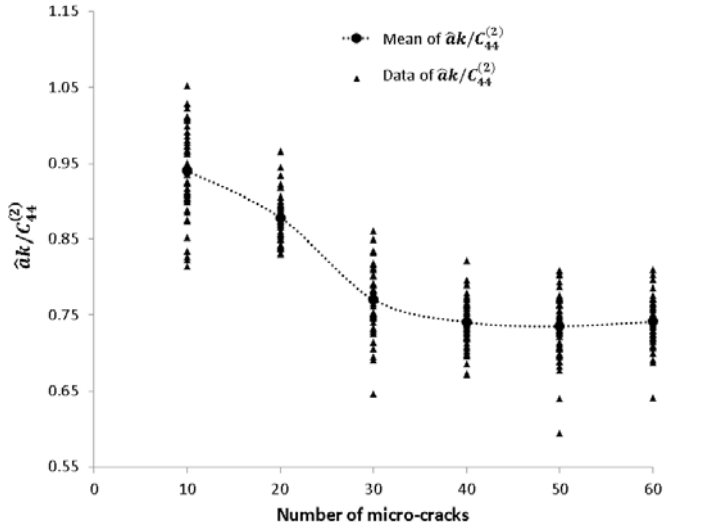

Figure 5. Scatter plots of the data of $\widehat{a}k/C_{44}^{(2)}$ and plots of the mean of the data for different values of M.

In Figures 2, 3, 4 and 5, the mean values of the non-dimensionalized coefficients decrease drastically as M increases from 10 to 40 and does not change very much for M greater than 40. The ranges of the scattered data of the non-dimensionalized coefficients remain more or less the same as M increases from 40 to 60 and are somewhat narrower than those for M less than 40.

The results in Figures 2, 3, 4 and 5 as well as further investigations conducted using other values of ρ and $\widehat{a}/h$, χ^2 distribution of different degrees of freedom and other materials in the layer and the half-space indicate that 40 micro-cracks per period interval of each interface are sufficient to homogenize the effective properties.

From all the investigations conducted, we also observe that the mean value of $\widehat{a}k/C_{44}^{(2)}$ (for interfaces containing electrically permeable micro-cracks) is very close to the corresponding mean value of $\widehat{a}k_{11}/C_{44}^{(2)}$ (for interfaces containing electrically impermeable micro-cracks). For a given M, the percentage difference between the two mean values is of the order 10^{-5} or smaller. Hence, only results involving interfaces damaged by electrically impermeable micro-cracks are presented in the parametric studies below.

6 Case studies

Some parametric studies on the effective properties of the interface are carried out here by using the micro-model proposed in Section 3. The studies conducted in this section assume that the micro-cracks on the interface are electrically impermeable. As pointed out in Section 4, the effective stiffness k for the interface containing electrically permeable micro-cracks is very close to the effective stiffness coefficient k_{11} for the interface containing electrically

impermeable micro-cracks.

For the estimation of the effective properties k_{ij}, a sample of 50 interfaces is generated randomly. The micro-crack length follows the $\chi^2(5)$ distribution. A period interval of the interface contains 40 micro-cracks.

The non-dimensionalized effective properties $\widehat{a}k_{11}/C_{44}^{(2)}$, $\widehat{a}k_{12}/\sqrt{C_{44}^{(2)}\epsilon_{11}^{(2)}}$, $\widehat{a}k_{21}/\sqrt{C_{44}^{(2)}\epsilon_{11}^{(2)}}$ and $\widehat{a}k_{22}/(-\epsilon_{11}^{(2)})$ are functions of the non-dimensionalized material constants $C_{44}^{(1)}/C_{44}^{(2)}$, $\epsilon_{11}^{(1)}/\epsilon_{11}^{(2)}$, $e_{15}^{(1)}/\sqrt{C_{44}^{(2)}\epsilon_{11}^{(2)}}$ and $e_{15}^{(2)}/\sqrt{C_{44}^{(2)}\epsilon_{11}^{(2)}}$, the interfacial damage ratio ρ and the non-dimensionalized width $h/\widehat{a}$ of the layer.

6.1 Effect of the piezoelectric coefficient $e_{15}^{(2)}/\sqrt{C_{44}^{(2)}\epsilon_{11}^{(2)}}$ of the half-space on the effective properties of the interface

Here we study the influence of $e_{15}^{(2)}/\sqrt{C_{44}^{(2)}\epsilon_{11}^{(2)}}$ on $\widehat{a}k_{11}/C_{44}^{(2)}$, $\widehat{a}k_{12}/\sqrt{C_{44}^{(2)}\epsilon_{11}^{(2)}}$, $\widehat{a}k_{21}/\sqrt{C_{44}^{(2)}\epsilon_{11}^{(2)}}$ and $\widehat{a}k_{22}/(-\epsilon_{11}^{(2)})$ for fixed values of the non-dimensionalized parameters $C_{44}^{(1)}/C_{44}^{(2)}$, $\epsilon_{11}^{(1)}/\epsilon_{11}^{(2)}$, $e_{15}^{(1)}/\sqrt{C_{44}^{(2)}\epsilon_{11}^{(2)}}$, ρ and $h/\widehat{a}$.

For a particular case, we take $e_{15}^{(1)}/\sqrt{C_{44}^{(2)}\epsilon_{11}^{(2)}} = 0$ (the thin layer is occupied by a dielectric material), $C_{44}^{(1)}/C_{44}^{(2)} = 1.5$, $\epsilon_{11}^{(1)}/\epsilon_{11}^{(2)} = 2$, $\rho = 0.5$ and $h/\widehat{a} = 1$. For this case, the mean values of the non-dimensionalized effective stiffness coefficients $\widehat{a}k_{11}/C_{44}^{(2)}$, $\widehat{a}k_{12}/\sqrt{C_{44}^{(2)}\epsilon_{11}^{(2)}}$ and $\widehat{a}k_{22}/(-\epsilon_{11}^{(2)})$ (from the statistical simulations) are plotted against $\log_{10}(e_{15}^{(2)}/\sqrt{C_{44}^{(2)}\epsilon_{11}^{(2)}})$ in Figures 6, 7 and 8 respectively. As may be expected, k_{21} is observed to be very close to k_{12}.

From Figures 6 and 8, as $e_{15}^{(2)}/\sqrt{C_{44}^{(2)}\epsilon_{11}^{(2)}}$ increases, the effective coefficients $\widehat{a}k_{11}/C_{44}^{(2)}$ and $\widehat{a}k_{22}/(-\epsilon_{11}^{(2)})$ appear to increase more drastically over $0.3 < e_{15}^{(2)}/\sqrt{C_{44}^{(2)}\epsilon_{11}^{(2)}} < 10$ (that is, for $-0.5 < \log_{10}(e_{15}^{(2)}/\sqrt{C_{44}^{(2)}\epsilon_{11}^{(2)}}) < 1$) than over

other ranges of $e_{15}^{(2)}/\sqrt{C_{44}^{(2)}\epsilon_{11}^{(2)}}$. For $0.3 < e_{15}^{(2)}/\sqrt{C_{44}^{(2)}\epsilon_{11}^{(2)}}$ and $e_{15}^{(2)}/\sqrt{C_{44}^{(2)}\epsilon_{11}^{(2)}} > 10$, $\widehat{a}k_{11}/C_{44}^{(2)}$ and $\widehat{a}k_{22}/(-\epsilon_{11}^{(2)})$ do not appear to vary much as $e_{15}^{(2)}/\sqrt{C_{44}^{(2)}\epsilon_{11}^{(2)}}$ increases.

In Figure 7, we observe that $\widehat{a}k_{12}/\sqrt{C_{44}^{(2)}\epsilon_{11}^{(2)}}$ has a local maximum at a certain value of $e_{15}^{(2)}/\sqrt{C_{44}^{(2)}\epsilon_{11}^{(2)}}$ and it appears to approach zero as $e_{15}^{(2)}/\sqrt{C_{44}^{(2)}\epsilon_{11}^{(2)}}$ becomes larger or tends to zero. In general, k_{12} and k_{21} are not zero. Hence, the assumption that k_{12} and k_{21} are zero, which may be found in many works on the macro-level generalized spring-like model for a weak interface, is not valid and it may probably be valid only under extreme situations such as if the coupling between the elastic and the electric fields in the half-space is either extremely small or extremely large.

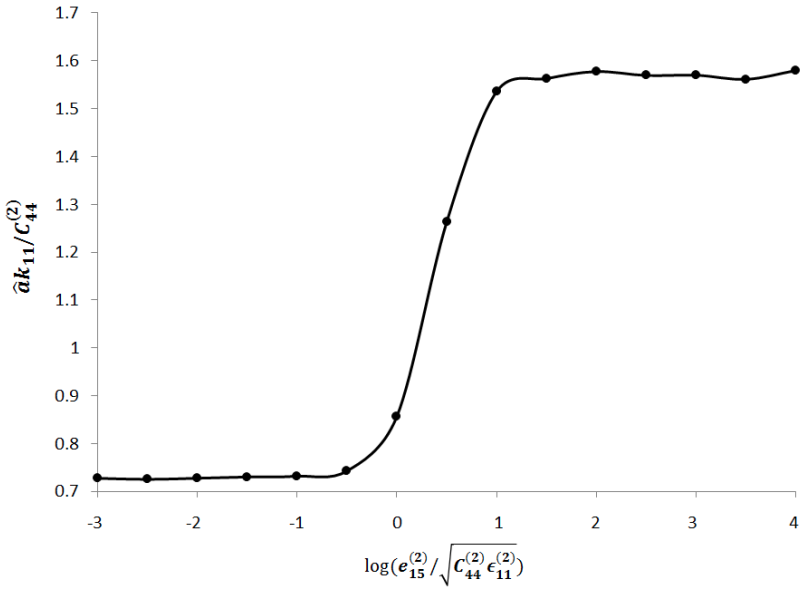

Figure 6. Plot of $\widehat{a}k_{11}/\sqrt{C_{44}^{(2)}\epsilon_{11}^{(2)}}$ against $\log_{10}(e_{15}^{(2)}/\sqrt{C_{44}^{(2)}\epsilon_{11}^{(2)}})$.

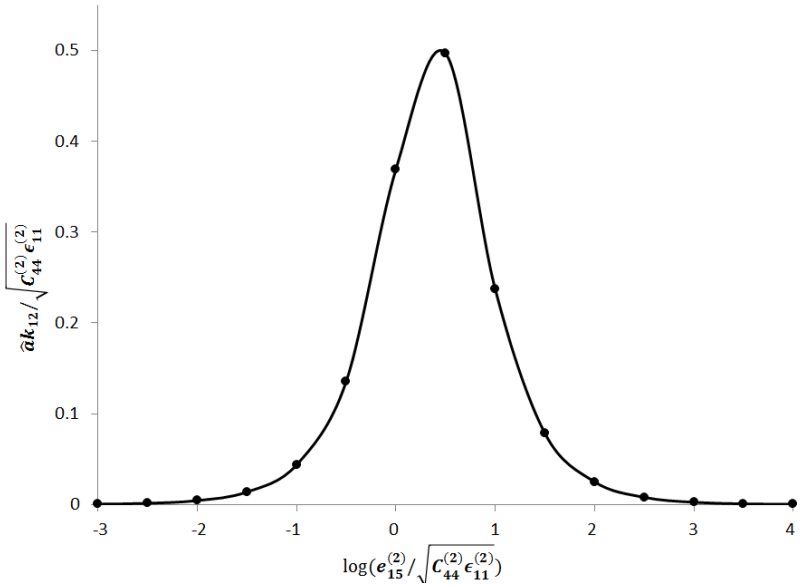

Figure 7. Plot of $\widehat{a}k_{12}/\sqrt{C_{44}^{(2)}\epsilon_{11}^{(2)}}$ against $\log_{10}(e_{15}^{(2)}/\sqrt{C_{44}^{(2)}\epsilon_{11}^{(2)}})$.

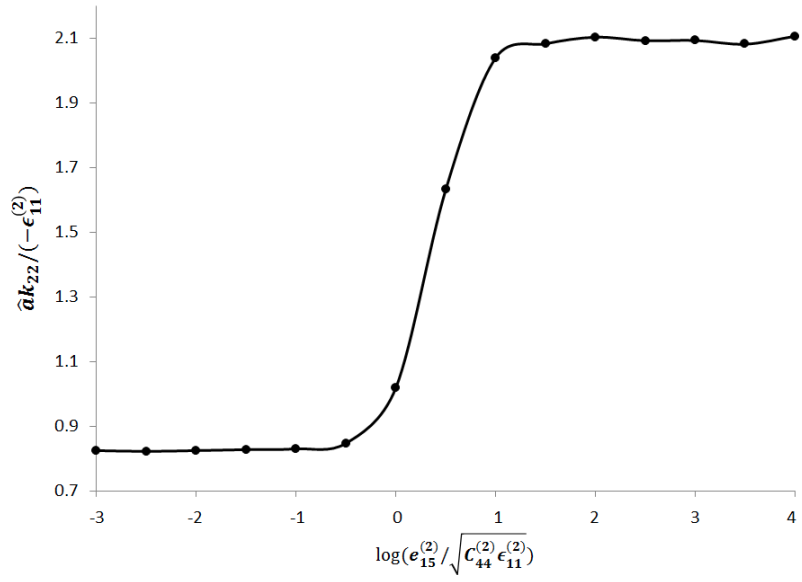

Figure 8. Plot of $\widehat{a}k_{22}/(-\epsilon_{11}^{(2)})$ against $\log_{10}(e_{15}^{(2)}/\sqrt{C_{44}^{(2)}\epsilon_{11}^{(2)}})$.

If the layer is piezoelectric, that is, $e_{15}^{(1)}/\sqrt{C_{44}^{(2)}\epsilon_{11}^{(2)}} \neq 0$, the variations of $\widehat{a}k_{11}/C_{44}^{(2)}$, $\widehat{a}k_{12}/\sqrt{C_{44}^{(2)}\epsilon_{11}^{(2)}}$ and $\widehat{a}k_{22}/(-\epsilon_{11}^{(2)})$ against $\log_{10}(e_{15}^{(2)}/\sqrt{C_{44}^{(2)}\epsilon_{11}^{(2)}})$ may not exhibit the same trends that as those in Figures 6, 7 and 8 (for the dielectric layer). For $C_{44}^{(1)}/C_{44}^{(2)} = 1.5$, $\epsilon_{11}^{(1)}/\epsilon_{11}^{(2)} = 2$, $\rho = 0.5$ and $h/\widehat{a} = 1$ and some selected values of $e_{15}^{(1)}/\sqrt{C_{44}^{(2)}\epsilon_{11}^{(2)}}$, we plot $\widehat{a}k_{11}/C_{44}^{(2)}$, $\widehat{a}k_{12}/\sqrt{C_{44}^{(2)}\epsilon_{11}^{(2)}}$ and $\widehat{a}k_{22}/(-\epsilon_{11}^{(2)})$ against $\log_{10}(e_{15}^{(2)}/\sqrt{C_{44}^{(2)}\epsilon_{11}^{(2)}})$ in Figures 9, 10 and 11 respectively. (Once again, k_{21} is found to be extremely close to k_{12}.) Unlike in Figures 6 and 8, the graphs of $\widehat{a}k_{11}/C_{44}^{(2)}$ and $\widehat{a}k_{22}/(-\epsilon_{11}^{(2)})$ in Figures 9 and 11 have local minimum values for $-0.5 < \log_{10}(e_{15}^{(2)}/\sqrt{C_{44}^{(2)}\epsilon_{11}^{(2)}}) < 1$. Also, unlike in Figure 7, the graph of $\widehat{a}k_{12}/\sqrt{C_{44}^{(2)}\epsilon_{11}^{(2)}}$ in Figure 10 does not have local maximum value for $-0.5 < \log_{10}(e_{15}^{(2)}/\sqrt{C_{44}^{(2)}\epsilon_{11}^{(2)}}) < 1$. It is obvious that $k_{12} \neq 0$ in general.

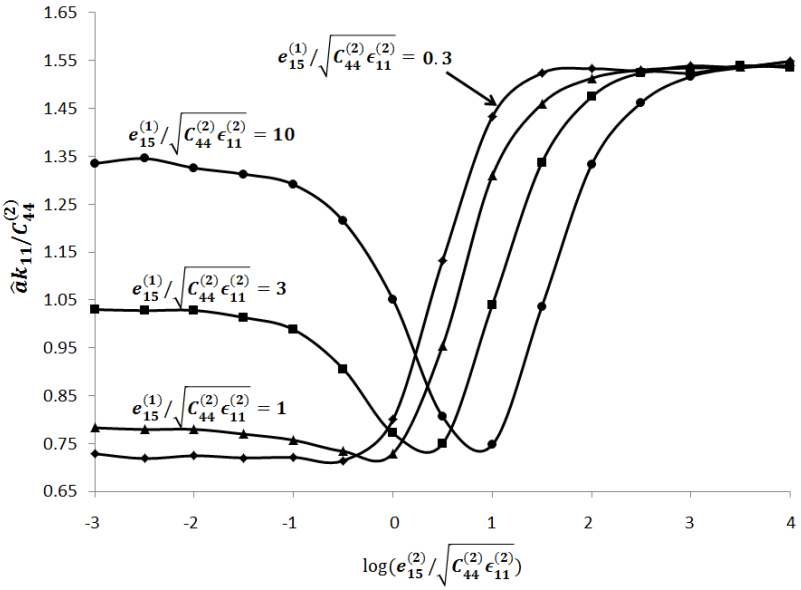

Figure 9. Plots of $\widehat{a}k_{11}/C_{44}^{(2)}$ against $\log_{10}(e_{15}^{(2)}/\sqrt{C_{44}^{(2)}\epsilon_{11}^{(2)}})$.

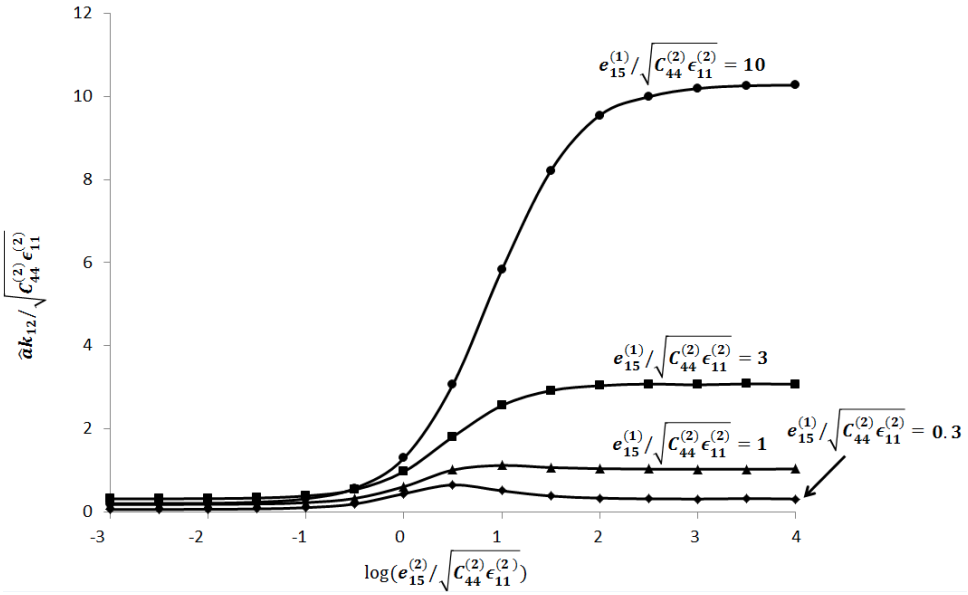

Figure 10. Plots of $\widehat{a}k_{12}/\sqrt{C_{44}^{(2)}\epsilon_{11}^{(2)}}$ against $\log_{10}(e_{15}^{(2)}/\sqrt{C_{44}^{(2)}\epsilon_{11}^{(2)}})$.

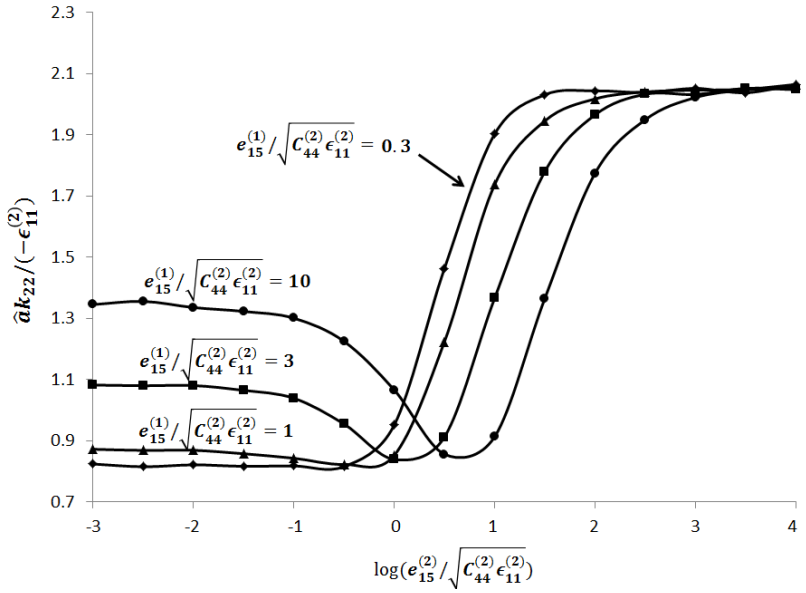

Figure 11. Plots of $\widehat{a}k_{22}/(-\epsilon_{11}^{(2)})$ against $\log_{10}(e_{15}^{(2)}/\sqrt{C_{44}^{(2)}\epsilon_{11}^{(2)}})$.

6.2 Effects of $C_{44}^{(1)}/C_{44}^{(2)}$ and $\epsilon_{11}^{(1)}/\epsilon_{11}^{(2)}$ on the effective properties of the interface between a dielectric layer and a piezoelectric half-space

For $e_{15}^{(1)}/\sqrt{C_{44}^{(2)}\epsilon_{11}^{(2)}} = 0$ (dielectric layer), $e_{15}^{(2)}/\sqrt{C_{44}^{(2)}\epsilon_{11}^{(2)}} = 1$, $\rho = 0.5$, $h/\widehat{a} = 1$ and some selected values of $\epsilon_{11}^{(1)}/\epsilon_{11}^{(2)}$, we plot $\widehat{a}k_{11}/C_{44}^{(2)}$, $\widehat{a}k_{12}/\sqrt{C_{44}^{(2)}\epsilon_{11}^{(2)}}$ and $\widehat{a}k_{22}/(-\epsilon_{11}^{(2)})$ against $\log_{10}(C_{44}^{(1)}/C_{44}^{(2)})$ in Figures 12, 13 and 14 respectively. As before, the difference between k_{12} and k_{21} is insignificant and hence only the plots of k_{12} are given.

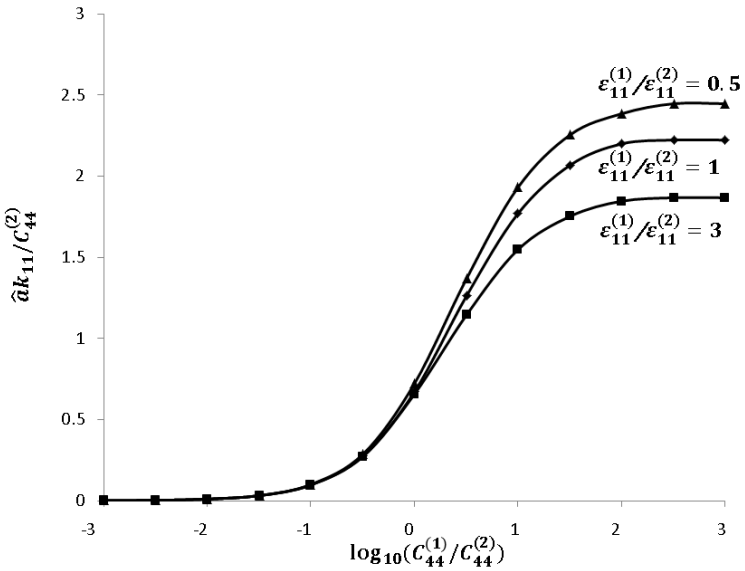

Figure 12. Plots of $\widehat{a}k_{11}/C_{44}^{(2)}$ against $\log_{10}(C_{44}^{(1)}/C_{44}^{(2)})$.

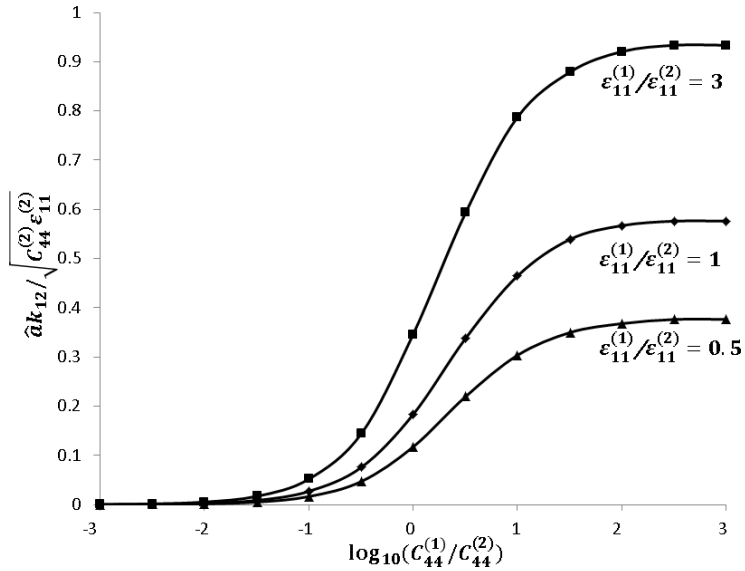

Figure 13. Plots of $\widehat{a}k_{12}/\sqrt{C_{44}^{(2)}\epsilon_{11}^{(2)}}$ against $\log_{10}(C_{44}^{(1)}/C_{44}^{(2)})$.

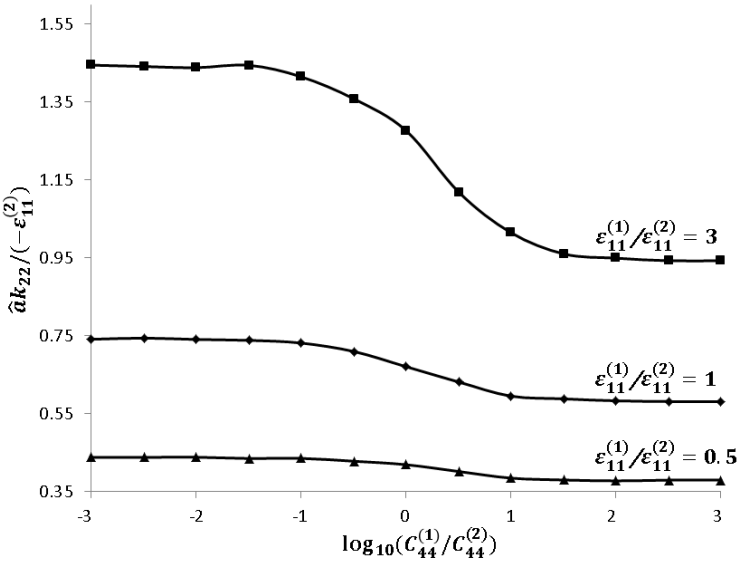

Figure 14. Plots of $\widehat{a}k_{22}/(-\epsilon_{11}^{(2)})$ against $\log_{10}(C_{44}^{(1)}/C_{44}^{(2)})$.

From Figures 12, and 13, both $\widehat{a}k_{11}/C_{44}^{(2)}$ and $\widehat{a}k_{12}/\sqrt{C_{44}^{(2)}\epsilon_{11}^{(2)}}$ appear to increase as $C_{44}^{(1)}/C_{44}^{(2)}$ increases (that is, as the strength of the thin layer relative to that of the half-space increases). In Figure 14, $\widehat{a}k_{22}/(-\epsilon_{11}^{(2)})$ seems to decrease as $C_{44}^{(1)}/C_{44}^{(2)}$ increases. It also appears that $\widehat{a}k_{11}/C_{44}^{(2)}$ and $\widehat{a}k_{12}/\sqrt{C_{44}^{(2)}\epsilon_{11}^{(2)}}$ tend to zero as $C_{44}^{(1)}/C_{44}^{(2)}$ becomes smaller. The effective coefficient $\widehat{a}k_{22}/(-\epsilon_{11}^{(2)})$ tends to a non-zero constant as $C_{44}^{(1)}/C_{44}^{(2)}$ approaches zero.

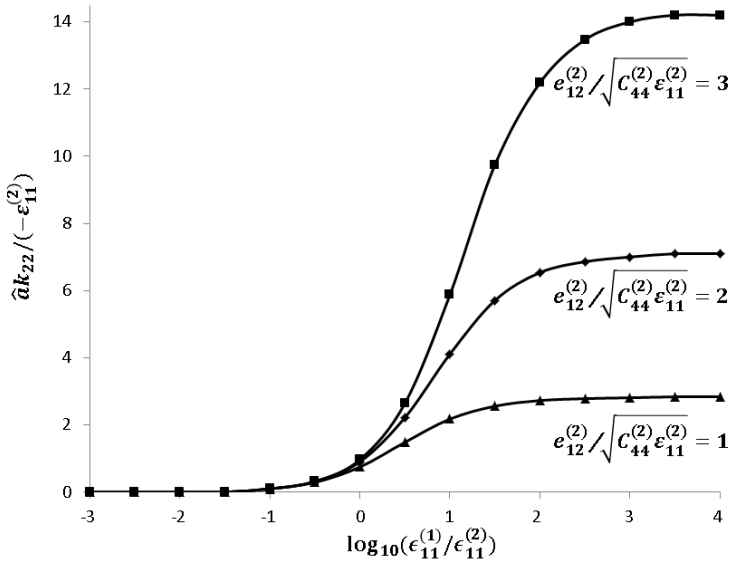

Figure 15. Plots of $\widehat{a}k_{22}/(-\epsilon_{11}^{(2)})$ against $\log_{10}(\epsilon_{11}^{(1)}/\epsilon_{11}^{(2)})$.

For a dielectric layer that is very soft relative to the half-space, it may be of interest to examine the effect of varying the non-dimensionalized dielectric constant $\epsilon_{11}^{(1)}/\epsilon_{11}^{(2)}$ on $\widehat{a}k_{22}/(-\epsilon_{11}^{(2)})$. In Figure 15, for $C_{44}^{(1)}/C_{44}^{(2)} = 0.001$, $e_{15}^{(1)}/\sqrt{C_{44}^{(2)}\epsilon_{11}^{(2)}} = 0$, $e_{15}^{(2)}/\sqrt{C_{44}^{(2)}\epsilon_{11}^{(2)}} = 1$, $\rho = 0.5$, $h/\widehat{a} = 1$ and some chosen values of $e_{15}^{(2)}/\sqrt{C_{44}^{(2)}\epsilon_{11}^{(2)}}$, we plot $\widehat{a}k_{22}/(-\epsilon_{11}^{(2)})$ against $\log_{10}(\epsilon_{11}^{(1)}/\epsilon_{11}^{(2)})$. From

the plots, for a given value of $e_{15}^{(2)}/\sqrt{C_{44}^{(2)}\epsilon_{11}^{(2)}}$, it is obvious that $\widehat{a}k_{22}/(-\epsilon_{11}^{(2)})$ increases with increasing $\epsilon_{11}^{(1)}/\epsilon_{11}^{(2)}$ and tend to a constant value as $\epsilon_{11}^{(1)}/\epsilon_{11}^{(2)}$ becomes larger and larger. Also, $\widehat{a}k_{22}/(-\epsilon_{11}^{(2)})$ tends to zero as $\epsilon_{11}^{(1)}/\epsilon_{11}^{(2)}$ approaches zero.

If we repeat all the calculations above by interchanging the values of $C_{44}^{(1)}/C_{44}^{(2)}$ and $\epsilon_{11}^{(1)}/\epsilon_{11}^{(2)}$, the value of $\widehat{a}k_{12}/\sqrt{C_{44}^{(2)}\epsilon_{11}^{(2)}}$ remains unchanged but the values of $\widehat{a}k_{11}/C_{44}^{(2)}$ and $\widehat{a}k_{22}/(-\epsilon_{11}^{(2)})$ are interchanged. (This is true in general, even for the case in which the layer is piezoelectric.) Thus, for $e_{15}^{(1)}/\sqrt{C_{44}^{(2)}\epsilon_{11}^{(2)}} = 0$, $e_{15}^{(2)}/\sqrt{C_{44}^{(2)}\epsilon_{11}^{(2)}} = 1$, $\rho = 0.5$, $h/\widehat{a} = 1$ and selected values of $C_{44}^{(1)}/C_{44}^{(2)}$, the plots of $\widehat{a}k_{12}/\sqrt{C_{44}^{(2)}\epsilon_{11}^{(2)}}$ against $\log_{10}(\epsilon_{11}^{(1)}/\epsilon_{11}^{(2)})$ are as given in Figure 13, with $C_{44}^{(1)}/C_{44}^{(2)}$ and $\epsilon_{11}^{(1)}/\epsilon_{11}^{(2)}$ in the figure replaced by $\epsilon_{11}^{(1)}/\epsilon_{11}^{(2)}$ and $C_{44}^{(1)}/C_{44}^{(2)}$ respectively. Similarly, plots of $\widehat{a}k_{11}/C_{44}^{(2)}$ and $\widehat{a}k_{22}/(-\epsilon_{11}^{(2)})$ are as given in Figures 12 and 14, with $C_{44}^{(1)}/C_{44}^{(2)}$, $\epsilon_{11}^{(1)}/\epsilon_{11}^{(2)}$, $\widehat{a}k_{11}/C_{44}^{(2)}$ and $\widehat{a}k_{22}/(-\epsilon_{11}^{(2)})$ in those figures replaced by $\epsilon_{11}^{(1)}/\epsilon_{11}^{(2)}$, $C_{44}^{(1)}/C_{44}^{(2)}$, $\widehat{a}k_{22}/(-\epsilon_{11}^{(2)})$ and $\widehat{a}k_{11}/C_{44}^{(2)}$ respectively. For a given $C_{44}^{(1)}/C_{44}^{(2)}$, the effective coefficients k_{12}, k_{21} and k_{22} are found to be close to zero if $\epsilon_{11}^{(1)}/\epsilon_{11}^{(2)}$ is extremely small.

6.3 Effect of the width of the layer on the effective properties of the interface

For $C_{44}^{(1)}/C_{44}^{(2)} = 1.5$, $e_{15}^{(1)}/\sqrt{C_{44}^{(2)}\epsilon_{11}^{(2)}} = 0$, $e_{15}^{(2)}/\sqrt{C_{44}^{(2)}\epsilon_{11}^{(2)}} = 0.25$, $\rho = 0.5$ and some chosen values of $\epsilon_{11}^{(1)}/\epsilon_{11}^{(2)}$, Figures 17, 18 and 19 give respectively the plots of $\widehat{a}k_{11}/C_{44}^{(2)}$, $\widehat{a}k_{12}/\sqrt{C_{44}^{(2)}\epsilon_{11}^{(2)}}$ and $\widehat{a}k_{22}/(-\epsilon_{11}^{(2)})$ against $\widehat{a}/h$. For a given value of $\epsilon_{11}^{(1)}/\epsilon_{11}^{(2)}$,the effective coefficients $\widehat{a}k_{11}/C_{44}^{(2)}$, $\widehat{a}k_{12}/\sqrt{C_{44}^{(2)}\epsilon_{11}^{(2)}}$ and $\widehat{a}k_{22}/(-\epsilon_{11}^{(2)})$ decrease as $\widehat{a}/h$ increases. This observation may be explained as follows.

As the width of the layer relative to the average half crack length becomes smaller, the edge of the layer interacts with the micro-cracks in such

a way that they become less stable. Thus, as $\widehat{a}/h$ increases, the generalized displacement jumps across the micro-cracks become larger, causing k_{11}, k_{12} and k_{22} to reduce in magnitude. The effect of the edge of the layer on the micro-cracks diminishes as $\widehat{a}/h$ increases (that is, as the width of the layer relative to the average half crack length increases). It follows that the values of $\widehat{a}k_{11}/C_{44}^{(2)}$, $\widehat{a}k_{12}/\sqrt{C_{44}^{(2)}\epsilon_{11}^{(2)}}$ and $\widehat{a}k_{22}/(-\epsilon_{11}^{(2)})$ tend to constant values as $\widehat{a}/h$ approaches zero, as is obvious in Figures 16, 17 and 18.

The observation above on how $\widehat{a}k_{11}/C_{44}^{(2)}$, $\widehat{a}k_{12}/\sqrt{C_{44}^{(2)}\epsilon_{11}^{(2)}}$ and $\widehat{a}k_{22}/(-\epsilon_{11}^{(2)})$ vary with $\widehat{a}/h$ is also true for other suitable values of the material constants $C_{44}^{(1)}/C_{44}^{(2)}$, $e_{15}^{(1)}/\sqrt{C_{44}^{(2)}\epsilon_{11}^{(2)}}$, $e_{15}^{(2)}/\sqrt{C_{44}^{(2)}\epsilon_{11}^{(2)}}$ and $\epsilon_{11}^{(1)}/\epsilon_{11}^{(2)}$and the damage ratio ρ of the interface.

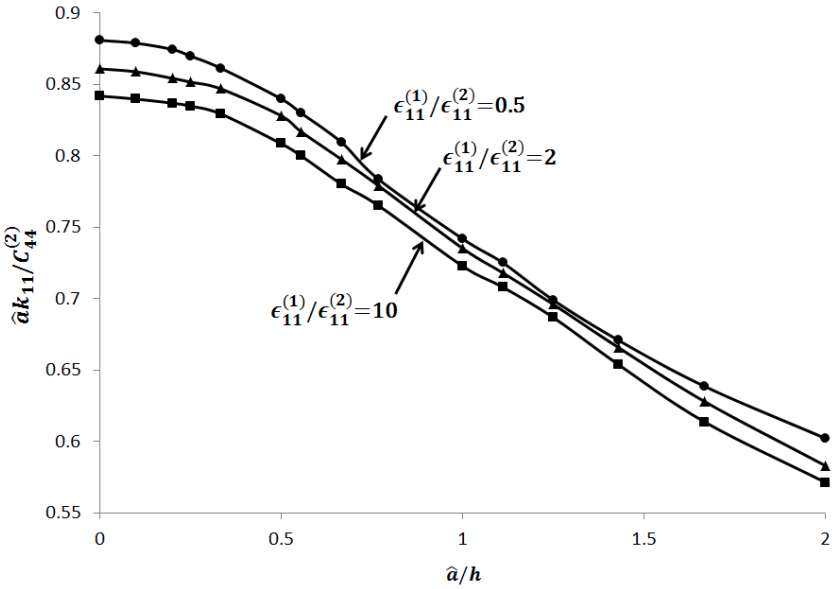

Figure 16. Plots of $\widehat{a}k_{11}/C_{44}^{(2)}$ against $\widehat{a}/h$.

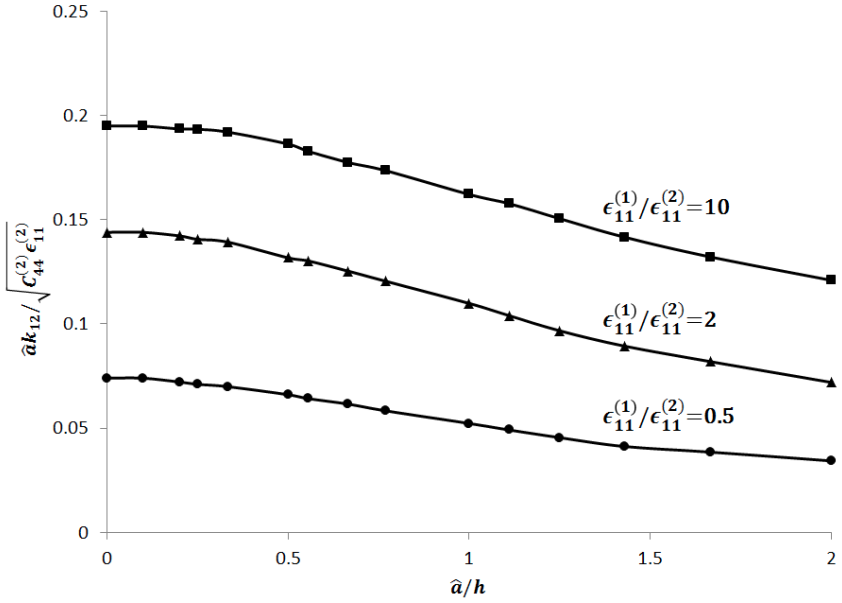

Figure 17. Plots of $\widehat{a}k_{12}/\sqrt{C_{44}^{(2)}\epsilon_{11}^{(2)}}$ against $\widehat{a}/h$.

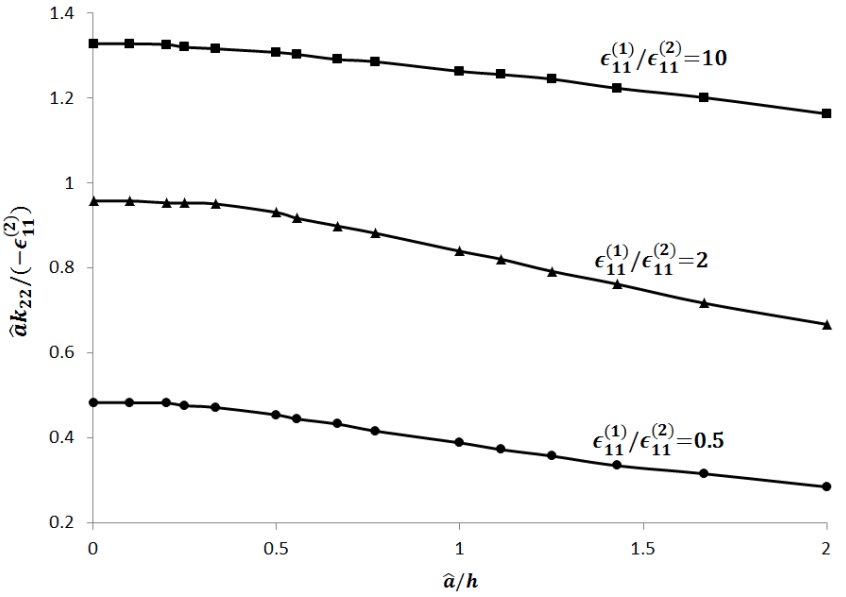

Figure 18. Plots of $\widehat{a}k_{22}/(-\epsilon_{11}^{(2)})$ against $\widehat{a}/h$.

7 Final remarks

The effective properties of micro-cracked interfaces between a layer and a half-space occupied by piezoelectric materials under antiplane deformations are estimated using a micro-statistical model. The model is formulated and solved in terms of hypersingular integral equations.

If the micro-cracks on the interface in question are electrically impermeable, the effective properties of the interface are characterized by k_{ij} $(i, j = 1, 2)$ as given in the macro-model defined by (6). For electrically permeable micro-cracks, the macro-model for the interface is given by (7), where the interface is characterized by only the effective stiffness coefficient k.

From our investigation on numerous specific cases, the effective stiffness coefficient k for an electrically permeable interface is numerically very close to the effective coefficient k_{11} for the corresponding electrically impermeable interface. The difference between effective coefficients k_{12} and k_{21} is numerically insignificant. In general, k_{12} and k_{21} are not zero. The assumption that k_{12} and k_{21} are zero, which is found in many papers on micro-models for interfaces between piezoelectric materials, may be valid under certain conditions only. From our studies on a specific case involving a dielectric layer, we find that k_{12} and k_{21} are close to zero, very small in magnitude compared to k_{11} and k_{22}, only if the coupling in the electric and elastic fields in the piezoelectric half-space is extremely weak or extremely strong.

We have examined in detail how the elastic moduli, the dielectric constants and the width of the layer affect the effective properties of the interface. The results obtained are intuitively acceptable.

In the present work, the micro-cracks are assumed to be either electrically impermeable or electrically permeable. It is possible to generalize the model to include micro-cracks with more realistic boundary conditions such as those given in Hao and Shen [6] and Zhao et al. [29]. However, the procedures for treating the more realistic conditions may be computationally more intensive. The micro-model here may also be extended to estimate macro-parameters in other problems involving imperfect spring-like interfaces, such as the effective dislocation-like or force-like interface parameters in the works of Wu et al. [26], Yu [27] and Yu et al. [28].

Acknowledgment

This research work is supported by the Singapore Ministry of Education Tier 1 Research Grant No. 81/15 awarded by Nanyang Technological University. The authors would like to thank the anonymous reviewers for their useful suggestions and comments which led to an improved version of this paper.

References

[1] Ang WT, *Hypersingular Integral Equations in Fracture Analysis*, Woodhead Publishing, Cambridge, 2013.

[2] Auld BA, *Acoustic plane waves in anisotropic solids*, Volume I, Wiley, 1973.

[3] Benveniste Y and Miloh T, Imperfect soft and stiff interfaces in two-dimensional elasticity, *Mechanics of Materials* **33** (2001) 309-323.

[4] Fan F and Sze KY, A micro-mechanics model for imperfect interface in dielectric materials, *Mechanics of Materials* **33** (2001) 363-370.

[5] Gurzadyan GG and Tzankov P, Dielectrics and Electrooptics, in *Springer Handbook of Condensed Matter and Materials Data* (pp. 817-901), Springer Berlin Heidelberg, 2005.

[6] Hao T and Shen H, A new electric boundary condition of electric fracture mechanics and its applications, *Engineering Fracture Mechanics* **47** (1994) 793-802.

[7] Hashin Z, The spherical inclusion with imperfect interface, *ASME Journal of Applied Mechanics* **58** (1991) 444-449.

[8] Jones JP and Whittier JS, Waves at a flexibly bonded interface, *Journal of Applied Mechanics* **34** (1967) 905-909.

[9] Li S and Gupta A, Peierls stress of a screw dislocation in a piezoelectric medium, *Applied Physics Letters* **85** (2004) 2211-2213.

[10] Li YD and Lee KY, Crack tip shielding and anti-shielding effects of the imperfect interface in a layered piezoelectric sensor, *International Journal of Solids and Structures* **46** (2009) 1736-1742.

[11] Li YD and Lee KY, Effect of an imperfect interface on the SH wave propagating in a cylindrical piezoelectric sensor, *Ultrasonics* **50** (2010) 473-478.

[12] Li YD and Lee KY, Interaction between an electrically permeable crack and the imperfect interface in a functionally graded piezoelectric sensor, *International Journal of Engineering Science* **47** (2009) 363-371.

[13] López-Realpozo JC, Rodríguez-Ramos R, Guinovart-Díaz R, Bravo-Castillero J and Sabina FJ, Transport properties in fibrous elastic rhombic composite with imperfect contact condition, *International Journal of Mechanical Sciences* **53** (2011) 98-107.

[14] Park KI, Son JH, Hwang GT, Jeong CK, Ryu J, Koo M, Choi I, Lee SH, Byun M, Wang ZL and Lee KJ, Highly-efficient, flexible piezoelectric PZT thin film nanogenerator on plastic substrates, *Advanced materials* **26** (2014) 2514-2520.

[15] Park KI, Xu S, Liu Y, Hwang GT, Kang SJL, Wang ZL and Lee KJ, Piezoelectric $BaTiO_3$ thin film nanogenerator on plastic substrates, *Nano Letters* **10** (2010) 4939-4943.

[16] Pilarski A and Rose JL, A transverse-wave ultrasonic oblique incidence technique for interfacial weakness detection in adhesive bonds, *Journal of Applied Physics* **63** (1988) 300–307.

[17] Rokhlin SI and Wang YJ, Analysis of boundary conditions for elastic wave interaction with an interface between two solids, *The Journal of the Acoustical Society of America* **89** (1991) 503–515.

[18] Tateyama Y, Morita Y, Tanaka K, Katayama T and Nakamachi E, Effects of $BaTiO_3$ piezoelectric thin film coating on activity of rat bone marrow cell, *IFMBE Proceedings of World Congress on Medical Physics and Biomedical Engineering* (2009) 279-281.

[19] Trolier-McKinstry S and Muralt P, Thin film piezoelectrics for MEMS, *Journal of Electroceramics* **12** (2004) 7-17.

[20] Wang X, Ang WT and Fan H, Micro-mechanics models for an imperfect interface under anti-plane shear load: Hypersingular integral formula-

tions, *Engineering Analysis with Boundary Elements* **36** (2012) 1856-1864.

[21] Wang X, Ang WT and Fan H, Hypersingular integral and integro-differential micromechanical models for an imperfect interface between a thin orthotropic layer and an orthotropic half-space under inplane elastostatic deformations, *Engineering Analysis with Boundary Elements* **52** (2015) 32-43.

[22] Wang X, Fan H and Ang WT, On micromechanical-statistical modeling of microscopically damaged interfaces under antiplane deformations, *International Journal of Solids and Structures* **51** (2014) 2327-2335.

[23] Wang X and Pan E, A moving screw dislocation interacting with an imperfect piezoelectric bimaterial interface, *physica status solidi* **244** (2007) 1940-1956.

[24] Wang X, Pan E and Roy AK, Scattering of antiplane shear wave by a piezoelectric circular cylinder with an imperfect interface, *Acta Mechanica* **193** (2007) 177-195.

[25] Wang X and Sudak LJ, A piezoelectric screw dislocation interacting with an imperfect piezoelectric bimaterial interface, *International Journal of Solids and Structures* **44** (2007) 3344-3358.

[26] Wu W, Xu S, Lv C, Xia R and Zhang J, Dislocation loop in isotropic bimaterial with linear spring-like imperfect interface, *Journal of Applied Mechanics* **83** (2016) 041005.

[27] Yu HY, A new dislocation-like model for imperfect interfaces and their effect on load transfer, *Composites Part A: Applied Science and Manufacturing* **29** (1998) 1057-1062.

[28] Yu HY, Wei YN and Chiang FP, Load transfer at imperfect interfaces—-dislocation-like model, *International journal of engineering science* **40** (2002) 1647-1662.

[29] Zhao MH, Guo ZH, Fan CY and Pan E, Electric and magnetic polarization saturation and breakdown models for penny shaped cracks in 3D magnetoelectroelastic media, *International Journal of Solids and Structures* **50** (2013) 1747-1754.